International Journal of Non-Linear Mechanics 149 (2023) 104324

Contents lists available at ScienceDirect

International Journal of Non-Linear Mechanics

journal homepage: www.elsevier.com/locate/nlm

Stable periodic oscillations in simple parallel-plate MEMS based on a family of graphene-like materials☆

D. Núñez [a,*], J. Galán-Vioque [b], L. Murcia [a,1]

[a] Departamento de Ciencias Naturales y Matemáticas. Pontificia Universidad Javeriana Cali, Facultad de Ingeniería y Ciencias, 760031, Cali, Colombia
[b] Instituto de Matemáticas de la Universidad de Sevilla and Departamento de Matemática Aplicada II, Escuela Técnica Superior de Ingeniería, Universidad de Sevilla, Sevilla, Spain

ARTICLE INFO

Keywords:
Graphene
MEMS
Periodic solutions
Linear stability
Lower and upper solutions method

ABSTRACT

In this paper we study the existence, multiplicity and the stability properties of lateral (positive) periodic oscillations in a class of simple parallel-plate MEM devices based on graphene and graphene-like materials with a non-constant T-periodic input voltage, which are modeled by Duffing equations. We also complete some partial results previously obtained in Kadyrov et al., (2021) for this kind of models and show analytically the existence of a positive asymptotically locally stable T-periodic oscillation, in particular for the graphene-based model. These results could be an approach to a design principle for stabilizing the device without an external controller by means of a tuning of the input voltage. Numerical continuation and simulations are also provided in order to illustrate theoretical results and to reveal the robustness of the graphene-based MEMS compared to the traditional ones.

1. Introduction

Microelectromechanical systems (MEMS) are micro-scale devices that integrates mechanical elements and electronics components on a common substrate (typically silicon) through micro fabrication technology, and as a whole system. These devices are employed as physical quantities sensors (e.g., inertia, pressure, mass, temperature, force and humidity sensors) and as actuators (e.g., RF switches, micro-grippers and thermal actuators). Furthermore, MEMS provide high performance, long-life and smart functionalities, and the achievement of complicated tasks in small places, everything by low fabrication and operational costs [1]. Hence, theoretical approaches based on mathematical modeling and simulations that allow the design of higher quality devices (with novel materials) and the optimization of those that are available, avoiding the former trial and error approach, could be of interest for researchers in MEMS.

It is worth to mention that there exist some novel materials that could be employed in the fabrication of MEMS leading to devices with a promising improved performance than the conventional ones. For example, the graphene is a mono-layer of carbon atoms that are tightly bounded and organized into a planar honeycomb lattice [2] with astonishing elastic, electromechanical, thermomechanical and electrical properties which make it suitable for applications in electronic devices like MEMS (see for example [2], [3], [4], [5], [6], [7], [8]). The elastic properties of this novel material has been studied in works like [9] and [10] within a framework of nonlinear elastic stress-strain response, and recently in [11] the authors considered the mechanical resonant modes in graphene and demonstrate a route for the generation of mechanical frequency combs in graphene resonators undergoing symmetry-breaking forces.

In this paper, we are interested in the stable periodic responses of a class of graphene-based devices. Specifically, we study from a mathematical point of view the stable nonlinear oscillatory behavior exhibited by electrostatic MEMS with a simple parallel-plate capacitor configuration [1] and which are based on graphene and graphene-like materials.

We consider a Duffing equation of the form

$$\ddot{x} + b\dot{x} + h(x) = \frac{F(t)}{(1-x)^2} \quad (x < 1), \tag{1}$$

with $b > 0$, $h \in C^1(\mathbb{R})$ and $F \in C(\mathbb{R}/T\mathbb{Z})$ a positive T-periodic function for some real $T > 0$.

The general Eq. (1) is inspired by the MEMS models with a parallel-plate capacitor structure and an AC–DC input voltage $V(t)$ such that $F(t) = \beta V^2(t)$, where $\beta > 0$ is a physical constant, and where $x(t)$ is

☆ Funding: This work was supported by the Pontificia Universidad Javeriana Cali Capital Semilla, Colombia project n° 020100750 and grants PGC2018-096265-B-I00, PGC2018-100680-B-C21 and P20-01160.

* Corresponding author.
E-mail addresses: denunez@javerianacali.edu.co (D. Núñez), jgv@us.es (J. Galán-Vioque), larry061198@javerianacali.edu.co (L. Murcia).

[1] Research assistant in the project 020100750.

https://doi.org/10.1016/j.ijnonlinmec.2022.104324
Received 17 October 2022; Accepted 1 December 2022
Available online 7 December 2022

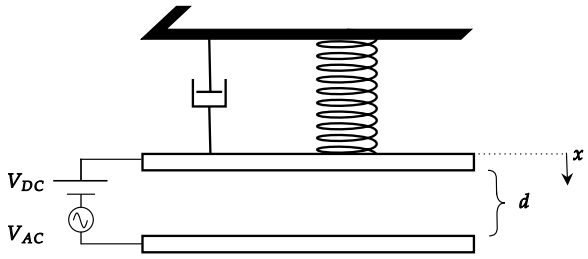

Fig. 1. Idealized parallel-plate capacitor for the graphene-based MEMS.

the normalized distance between plates in time t (see Fig. 1 for an illustration). We remark that devices with this configuration consist in two rectangular parallel electrodes; one of them fixed and the other one movable in the transversal direction. As a consequence of the driving voltage there is an attracting force generated between the two electrodes called electrostatic force which tends to deflect the movable electrode. This last one is usually a flexible structure that generates an elastic restoring force that acts on the opposite direction of the electrostatic force (see [1] for more details). The constant input voltage for which the forces are balanced is known as the pull-in voltage. Beyond this constant voltage the plates collide.

Hence the right side of (1) represents the electrostatic force between plates and the function h is such that $f_e = -h$ represents the restoring force due to, for example, the manufacturing materials employed in MEMS structures (see [1] for some classical MEMS models with ODEs). Then, we postulate the existence of a dimensional maximum deformation of the micro structure under stress, which leads to a non-dimensional strain parameter $\mu_e > 0$. This means that f_e is restoring whenever $|x| < \mu_e$, i.e., $xh(x) > 0$ if $x \neq 0$, $f_e(\pm\mu_e) = 0$, and f_e is not recovering when $|x| > \mu_e$, i.e., the sign of f_e is the same of the deformation: $xh(x) < 0$ if $|x| > \mu_e$. Thus, with this in mind we assume the following general hypotheses over the function h:

H1. h is odd (we are assuming that the magnitude of the restoring force is the same by axial compression or expansion).
H2. $\exists\ \mu_e > 0$: $h(\mu_e) = 0$, $h > 0$ on $]0, \mu_e[$ and $h'(\mu_e) < 0 < h'(0)$.
H3. $h \in C^1(\mathbb{R}) \cap C^2(]0, \mu_e[)$ and $h'' \leq 0$ on $]0, \mu_e[$.

We set the class of functions $\mathcal{H}$ like those real-valued functions verifying hypotheses H1, H2 and H3. Hence, in this work we are interested in finding T-periodic solutions of (1) whenever $h \in \mathcal{H}$, with range in $]-\mu_e, \mu_e[$. Henceforth, we shall consider that any solution of (1) whose range is not included in $]-\mu_e, \mu_e[$ is physical meaningless.

In particular for the non-dimensional graphene-based model first introduced in [12] we have $h(x) = x - \alpha|x|x$ and $\mu_e = \frac{1}{\alpha}$ for $\alpha > 0$ in (1). It is not difficult to check that $h \in \mathcal{H}$. We remark that α is a constant parameter associated to the mechanical properties of the graphene and the geometry of the device. Thus, the non-dimensional graphene-based model is given by

$$\ddot{x} + b\dot{x} + x - \alpha|x|x = \frac{\beta V^2(t)}{(1-x)^2}. \tag{2}$$

In [12] the authors study some periodic solutions for (1) but they do not search for the corresponding stability properties. We remark that these periodic solutions are typically unstable (for more details see first paragraph, page 6). In this paper we focus on get the stable periodic solutions of this model. Thus the main objective of this paper is to complete the study given in [12] providing analytical results about multiplicity, existence and stability properties of periodic oscillations of general Eq. (1). In particular, we will focus on getting stable periodic solutions of this model.

Next, we provide some preliminaries. Let us define

$$F_m := \min F, \quad F_M := \max F, \tag{3}$$

$$\mu_1 := \min\{1, \mu_e\}, \tag{4}$$

and a function $\phi(x)$ called the *auxiliary function* associated to (1) by

$$\phi(x) := (1-x)^2 h(x) \quad (x < 1).$$

1.1. The Lower and Upper Solutions approach

It is worthy to mention that the problem of finding T-periodic solutions of (1) is equivalent to solve the periodic boundary problem given by (1) along with the boundary conditions $x(0) = x(T)$, $\dot{x}(0) = \dot{x}(T)$. Thus, in order to find T-periodic solutions of (1) we can follow the Lower and Upper Solutions approach (see [13]). Specifically, we shall use constant lower and upper solutions of the periodic boundary problem associated to (1).

A constant function $u(t) \equiv \gamma$ is said to be a lower solution of (1) if for all $t \in \mathbb{R}$

$$\ddot{u} + b\dot{u} + h(u) \geq \frac{F(t)}{(1-u)^2} \iff \phi(\gamma) \geq F(t). \tag{5}$$

The definition of upper solution is similar but reversing the inequality in (5). Thus an upper solution $u(t) \equiv \eta$ of (1) satisfies that for all $t \in \mathbb{R}$

$$\phi(\eta) \leq F(t). \tag{6}$$

We notice that, whenever the inequality (5) (resp. (6)) is strict, then γ (resp. η) is called a strict lower solution (resp. strict upper solution) of (1).

Remark 1. *The theory basically says that if we have γ and η a pair of constant lower and upper solutions of (1) respectively, such that $\gamma < \eta$, then there exists a T-periodic solution $x_0(t)$ of (1) which satisfies for all $t \in \mathbb{R}$*

$$\gamma \leq x_0(t) \leq \eta.$$

This claim follows as a consequence of Theorem 5.3 (chapter 1) in [13], because we have a problem with a linear dependence on the derivative $\dot{x}$ and the function $g(t,x) = h(x) - \frac{F(t)}{(1-x)^2}$ is continuous on its domain.

Remark 2. *Let us assume that γ and η are a pair of constant lower and upper solutions of (1) such that $\eta < \gamma$ (reversed order), that the coefficient $b > 0$ is appropriately bounded and that $g(t,x)$ has a continuous partial derivative with respect to x verifying for all $(t,x) \in \mathbb{R} \times]\eta, \gamma[$: $g_x(t,x) < \left(\frac{\pi}{T}\right)^2$. Then there exists a $T-periodic$ solution $v_0(t)$ of (1) which satisfies for all $t \in \mathbb{R}$*

$$\eta \leq v_0(t) \leq \gamma.$$

This result is consequence of a particular case of Theorem 3.2 (chapter 5) in [13].

We notice that (5) and (6) are equivalent to $\phi(\gamma) \geq F_M$ and $\phi(\eta) \leq F_m$ respectively. In particular, the solutions of equation

$$\phi(x) = F_M, \tag{7}$$

are lower solutions of (1), and the solutions of equation

$$\phi(x) = F_m, \tag{8}$$

are upper solutions of (1). These lower and upper solutions are called non-strict constant lower and upper solutions.

Next we study the constant lower and upper solutions for (1). First we prove that if $h \in \mathcal{H}$ then the associated *auxiliary function* ϕ is unimodal on $[0, \mu_1]$ (Lemma 1) what allow us know the distribution of positive non-strict constant lower and upper solutions (Lemma 2).

Lemma 1. *If $h \in \mathcal{H}$ then ϕ has the following properties:*

(i) $\phi \in C^1(\mathbb{R}) \cap C^2(]0, \mu_1[)$ *and verifies that* $\phi > 0$ *on* $]0, \mu_1[$ *with* $\phi(0) = \phi(\mu_1) = 0$.

(*ii*) *ϕ has a unique critical point $c \in]0,\mu_1[$ and thus $\phi'(x) > 0\ \forall x \in [0,c[$ and $\phi'(x) < 0\ \forall x \in]c,\mu_1[$.*

Proof. Claim (*i*) is obvious from the properties of h. Now let us consider the derivative

$$\phi'(x) = (1-x)^2 h'(x) - 2(1-x)h(x).$$

Then $x \in]0,\mu_1[$ is a critical point of ϕ if and only if

$$\Phi(x) := \frac{h'(x)}{h(x)} - \frac{2}{1-x} = 0. \tag{9}$$

Since $h(0) = 0$, $h > 0$ on $]0,\mu_e[$ and $h'(\mu_e) < 0 < h'(0)$ then

$$\lim_{x\to 0^+} \Phi(x) = \infty, \quad \lim_{x\to \mu_1^-} \Phi(x) = -\infty. \tag{10}$$

On the other hand, Φ is strictly decreasing on $]0,\mu_1[$. Effectively,

$$\Phi'(x) = \frac{h''(x)h(x) - (h'(x))^2}{h^2(x)} - \frac{2}{(1-x)^2},$$

and thus $\Phi' < 0$ on $]0,\mu_1[$, because $h'' \le 0$ on $]0,\mu_e[$ and $h > 0$ on $]0,\mu_e[$.

In consequence, Φ has a unique root $c \in]0,\mu_1[$. Clearly, from (9) and (10) we have that $\Phi(x) > 0$ on $]0,c[$ and $\Phi(x) < 0$ on $]c,\mu_1[$. Claim (*ii*) then follows since $\phi'(0) = h'(0)$. □

Now, let us define

$$\phi_M := \max_{x\in]0,\mu_1[} \phi(x) = \phi(c) > 0, \tag{11}$$

where c is the unique critical point of ϕ given in Lemma 1. Thus, the following lemma provides information about the solutions of (7) and (8) on the domain $]-\mu_e,\mu_1[$.

Lemma 2 (*Existence of Non-Strict Lower and Upper Solutions for (1)*)**.** *Let $h \in \mathcal{H}$ and assume that $F_M \le \phi_M$ in (1). Then Eq. (7) has at most two roots $0 < \ell_1 \le \ell_2$ on $]-\mu_e,\mu_1[$, and Eq. (8) has at most two roots $0 < u_1 \le u_2$ on $]-\mu_e,\mu_1[$ which verify that*

$$0 < u_1 \le \ell_1 \le c \le \ell_2 \le u_2.$$

If F is a non-constant function then $u_1 < \ell_1$ and $\ell_2 < u_2$. Moreover, if $F_M < \phi_M$ then both ℓ_i and both u_i are different.

Proof. From Lemma 1 we have that ϕ is increasing on $[0,c[$ and decreasing on $]c,\mu_1[$. Thus, if $F_M = \phi_M$ then one has that $\ell_1 = \ell_2 = c$, and if $F_M < \phi_M$, by the Intermediate Value Theorem applied to the function ϕ restricted to the intervals $]0,c[$ and $]c,\mu_1[$ respectively, we obtain the existence of $\ell_1 \in]0,c[$ and $\ell_2 \in]c,\mu_1[$ such that $\phi(\ell_1) = F_M = \phi(\ell_2)$. Notice that we have at most ℓ_1 and ℓ_2 since ϕ is a strictly monotonic function on each interval. An analogous reasoning shows the existence of $0 < u_1 < u_2$ such that $\phi(u_1) = F_m = \phi(u_2)$ since $0 < F_m \le F_M < \phi_M$. The order of the roots $u_1 \le \ell_1 < c < \ell_2 \le u_2$ follows from the monotonic character of function ϕ on the intervals $]0,c[$ and $]c,\mu_1[$, with the strict inequalities holding whenever $F_m < F_M$. Finally, the reader should notice that since $0 < F_m$ and $\phi < 0$ on $]-\mu_e,0[$, then we have no more roots of Eqs. (7) and (8) besides those already provided. □

1.2. The main results

We assume from now on that F is non-constant and notice that the preceding approach lead us to a first result about the existence of T-periodic solutions of (1) whenever we take $h \in \mathcal{H}$ and $0 < b < b^*$, $0 < T < T^*$ for certain computable bounds b^* and T^* (see for instance Theorem 1 for the graphene model). Thus, if $F_M \le \phi_M$ then there exist at least two T-periodic solutions of (1), $x_0(t)$ and $v_0(t)$, such that for all $t \in \mathbb{R}$

$$0 < u_1 \le v_0(t) \le \ell_1 \le \ell_2 \le x_0(t) \le u_2 < \mu_1,$$

where u_i and ℓ_i are *a posteriori* bounds of the solutions that are given by Lemma 2. Moreover, it is possible to prove that v_0 is asymptotically locally stable by means of an additional restriction over b that is imposed by the linearization technique (Liapounoff-Zukovskii criteria for Hill's equations).

Perhaps, this is the first analytical result about stability for periodic solutions for the general model (1) introduced by Kadyrov et al. in [12]. Indeed, the authors in [12] do not provide any analytical results about the stability for the periodic solutions obtained in Theorem 1 there, and only performed numerical examples. Furthermore, the periodic solution presented in that paper is normally unstable, because it is obtained via well ordered lower and upper solutions (see Proposition 3.1 and subsequent Remark in [14]), hence it corresponds to the solution $x_0(t)$, forgetting the most crucial periodic solution $v_0(t)$ which will be typically stable. Thus we aim to complete the study presented in [12] and to provide an analysis about stability properties of periodic solutions of the general differential Eq. (1), in particular, the implications over the graphene model (2).

Concretely, when this result is applied to a graphene-based MEMS modeled by (2), it is not difficult to obtain the following result (Theorem 1). First we provide some necessary definitions. Let us consider

$$V_{max} = \max_{t\in[0,T]} V(t), \quad V_{min} = \min_{t\in[0,T]} V(t),$$

and the *auxiliary function* associated to the graphene-base model given by

$$\phi_\alpha(x) = (1-x)^2(x - \alpha|x|x).$$

Assume that $\beta V_{max}^2 < \max_{]0,\mu_1[} \phi_\alpha$ and for $s \in \left]0,(\frac{\pi}{T})^2\right[$ let us define $G : \left[s,(\frac{\pi}{T})^2\right] \to \mathbb{R}$ as

$$G(\ell) = \frac{\ell - s}{\sqrt{\ell}} \cot\sqrt{\ell}\left(\frac{T}{2}\right), \tag{12}$$

whenever $s \le \ell \le \left(\frac{\pi}{T}\right)^2$. Thus, G is a continuous non-negative function that is zero only on the boundary. We remark that function G arises from the methodology in order to employ Theorem 3.2 in [13] (chapter 5). Then, if u_1 and ℓ_1 denote the positive roots given by Lemma 2 with the *auxiliary function* ϕ_α for the graphene model and $F(t) = \beta V^2(t)$, we set

$$s^* = \frac{\phi'_\alpha(u_1)}{(1-u_1)^2},$$

and define the following quantities

$$b(s^*) := \max_{\ell\in\left[s^*,(\frac{\pi}{T})^2\right]} G(\ell), \quad T^* = \pi\frac{(1-c_\alpha)}{\sqrt{\phi'_\alpha(u_1)}},$$

$$b^* = \min\left\{2\frac{\sqrt{\phi'_\alpha(\ell_1)}}{(1-\ell_1)}, b(s^*)\right\},$$

for $0 < T \le T^*$, where c_α is the unique critical point of ϕ_α given by Lemma 1.

Theorem 1. *Assume that $V_{max}^2 < \frac{\phi_\alpha(c_\alpha)}{\beta}$, $0 < T \le T^*$ and $0 < b < b*$. Then there exist at least two T-periodic solutions $x_0(t)$ and $v_0(t)$ of (2) such that for all $t \in [0,T]$*

$$0 < v_0(t) < x_0(t),$$

where $v_0(t)$ is asymptotically locally stable. Additionally, if we assume that

$$1 - 2\beta V_{min}^2 \le \left(\frac{\pi}{T}\right)^2 + \frac{b^2}{4}, \tag{13}$$

then $x_0(t)$ and $v_0(t)$ are the only positive T-periodic solutions of (2) and $x_0(t)$ is unstable.

The main purpose of this work is to provide a new general result about the existence, multiplicity, and the stability properties of T-periodic solutions of (1) with lesser restrictive conditions than those imposed in Theorem 1. Hence, we shall complete the partial results for (1) stated in [12]. For that purpose we will combine the known multiplicity results for periodic solutions of a Duffing equation with convex potential (see [15]) and some results that relate the asymptotic stability of periodic solutions with Topological Degree (see [16,17]), in order to obtain results for the existence of asymptotically stable periodic solutions of (1) (see Section 2).

Next we present some necessary preliminaries in order to introduce the main result of this work.

Let $p \in [1,\infty]$. Then we define $K(p,T)$ as the best Sobolev constant in the inequality

$$C\|u\|_p^2 \leq \|\dot{u}\|_2^2,$$

for all $u \in H_0^1(0,T)$, which is explicitly given by (see [18,19])

$$K(p,T) = \begin{cases} \dfrac{2\pi}{pT^{1+\frac{2}{p}}}\left(\dfrac{2}{2+p}\right)^{1-\frac{2}{p}}\left(\dfrac{\Gamma(\frac{1}{p})}{\Gamma(\frac{1}{2}+\frac{1}{p})}\right)^2, & \text{if } 1 \leq p < \infty, \\ \dfrac{4}{T}, & \text{if } p = \infty. \end{cases}$$

Now, we are able to state our main result about the existence and the stability properties of periodic solutions of the general Eq. (1).

Theorem 2. *Consider Eq. (1), let $h \in \mathcal{H}$ and $C_0 = \max\{h'(0), 2F_M\}$ for F non-constant. Assume that $F_M < \phi_M$ and that there exists some $p \in [1,\infty]$ such that*

$$\|a\|_p < \left(1 + \frac{T^2b^2}{4\pi^2}\right) K(2p^*,T), \tag{14}$$

where $a(t) := C_0 - 2F(t)$ and p, p^* are conjugate exponents. Then (1) has exactly two positive T-periodic solutions $x(t)$ and $v(t)$ verifying that $v(t) < x(t)$ for all $t \in [0,T]$. Moreover, $v(t)$ is asymptotically locally stable and $x(t)$ is unstable.

Remark 3. *Theorem 2 completes the study about positive T-periodic solutions of (1) by giving information about their stability properties and multiplicity. In fact, Theorem 2 shows that, under certain conditions, (1) admits exactly two positive T-periodic solutions, one of them is asymptotically locally stable and the other is unstable.*

Next corollary provides a more practical condition than (14) for the cases $p = \infty$ and $p = 1$.

Corollary 1. *Let h and C_0 be as in Theorem 2. Assume that some of the following conditions holds:*

(a)

$$\frac{C_0}{2} - \frac{\pi^2}{2T^2}\left(1 + \frac{T^2b^2}{4\pi^2}\right) < \phi_M,$$

and

$$F_m,\ F_M \in \left]\frac{C_0}{2} - \frac{\pi^2}{2T^2}\left(1 + \frac{T^2b^2}{4\pi^2}\right), \phi_M\right[.$$

(b) $F_M < \phi_M$ *and*

$$\overline{F} > \frac{C_0}{2} - \frac{2}{T^2}\left(1 + \frac{T^2b^2}{4\pi^2}\right),$$

where $\overline{F} := \frac{1}{T}\int_0^T F(t)dt$.

Then conclusion in Theorem 2 is also true.

In particular, we obtain the following results for the graphene-based MEMS model.

Theorem 3. *Assume for Eq. (2) that $V_{max}^2 < \frac{\phi_\alpha(c_\alpha)}{\beta}$ and that there exists $p \in [1,\infty]$ such that*

$$\left\|1 - 2\beta V^2(t)\right\|_p < \left(1 + \frac{T^2b^2}{4\pi^2}\right) K(2p^*,T), \tag{15}$$

where p, p^* are conjugate exponents. Then (2) has exactly two T-periodic solutions $x_0(t)$ and $v_0(t)$ such that for all $t \in [0,T]$

$$0 < v_0(t) < x_0(t),$$

where $v_0(t)$ is asymptotically locally stable and $x_0(t)$ is unstable.

Remark 4. *Theorem 3 provides a more complete insight about T-periodic oscillations in the graphene-based MEMS than the one obtained in Theorem 2 stated in [12].*

A more practical condition than (15) for the cases $p = \infty$ and $p = 1$ is given in the following corollary.

Corollary 2. *Let $\eta_1 := \frac{1}{2\beta} - \frac{\pi^2}{2\beta T^2}\left(1 + \frac{T^2b^2}{4\pi^2}\right)$ and $\eta_2 := \frac{\phi_\alpha(c_\alpha)}{\beta}$. Assume that for Eq. (2) some of the next conditions holds:*

(a) $\eta_1 < \eta_2$, $V_{min}^2 > \eta_1$ *and* $V_{max}^2 < \eta_2$.
(b) $V_{max}^2 < \eta_2$ *and* $\|V\|_2^2 > \frac{T}{2\beta} - \frac{2}{\beta T}\left(1 + \frac{T^2b^2}{4\pi^2}\right)$.

Then conclusion in Theorem 3 is also valid.

Remark 5. *We notice that Theorem 1 and Corollary 2 provide results about the existence, multiplicity and the stability properties of positive T-periodic solutions of (2). In this sense, Corollary 2 requires less restrictive conditions than those imposed in Theorem 1 (with all conditions assumed). Effectively, if we assume that all hypotheses in Theorem 1 hold then condition (a) in Corollary 2 is satisfied. More precisely, $\eta_1 < \eta_2$ is equivalent to have $1 - 2\phi_\alpha(c_\alpha) < \frac{\pi^2}{T^2} + \frac{b^2}{4}$ which is true because from hypotheses in Theorem 1 we have $\beta V_{min}^2 < \phi_\alpha(c_\alpha)$ and (13) holds. Besides, $V_{min}^2 > \eta_1$ is equivalent to (13) and $V_{max}^2 < \eta_2$ is a direct assumption in Theorem 1.*

2. Proofs

Proof of Theorem 2. In order to prove this result, we consider three steps. First we check the multiplicity of positive T-periodic solutions of (1). Next we shall prove the existence of constant lower and upper solutions for (1). Finally we shall prove the existence and stability properties of positive T-periodic solutions of (1).

Multiplicity: We notice that $a(t) = C_0 - 2F(t) \in L^1(0,T)$ and is T-periodic because $F \in C(\mathbb{R}/T\mathbb{Z})$. Furthermore, because $C_0 \geq 2F_M > 0$ and F is non-constant we have that $a(t) > 0$ almost everywhere on $\mathbb{R}$. Now let us define $g(t,x) = h(x) - \frac{F(t)}{(1-x)^2}$ so that (1) turns into $\ddot{x} + b\dot{x} + g(t,x) = 0$. Then $g \in C^{0,1}(\mathbb{R}/T\mathbb{Z} \times]0,\mu_1[)$ and we have that

$$g_x(t,x) = h'(x) - \frac{2F(t)}{(1-x)^3} \quad \text{and} \quad g_{xx}(t,x) = h''(x) - \frac{6F(t)}{(1-x)^4}.$$

Since $h \in \mathcal{H}$, $F(t) > 0$ for all $t \in \mathbb{R}$, $\mu_1 \leq \mu_e$ and $C_0 \geq h'(0) > 0$ it follows that for all $t \in \mathbb{R}$ and $x \in]0,\mu_1[$

$$g_x(t,x) \leq h'(0) - 2F(t) \leq a(t) \quad \text{and} \quad g_{xx}(t,x) < 0.$$

Thus, from hypothesis (14) and Lemma 4 in Appendix we conclude that (1) has at most two non-trivial T-periodic solutions with range in $]0,\mu_1[$ (positive solutions).

Strict constant lower and upper solutions: Since $h \in \mathcal{H}$, $F_M < \phi_M$ and F is a non-constant function, it follows from Lemma 2 that there exist non-strict constant lower and upper solutions for (1), ℓ_1, ℓ_2 and u_1, u_2 respectively, such that

$$0 < u_1 < \ell_1 < c < \ell_2 < u_2 < \mu_1,$$

whenever $x \in]-\mu_e,\mu_1[$. Moreover, $\phi(u_1) = \phi(u_2) = F_m$ and $\phi(\ell_1) = \phi(\ell_2) = F_M$. From Lemma 1 we know that ϕ is a positive continuous function on $]0,\mu_1[$ which is increasing ($\phi' > 0$) on $]0,c[$ and decreasing

($\phi' < 0$) on $]c, \mu_1[$. Thus, for $i = 1, 2$ there exist positive and small enough constants δ_i, ζ_i such that

$$0 < U_1 < L_1 < c < L_2 < U_2 < \mu_1,$$

where $U_1 = u_1 - \delta_1$, $U_2 = u_2 + \delta_2$, $L_1 = \ell_1 + \zeta_1$ and $L_2 = \ell_2 - \zeta_2$ which verify

$$\phi(U_1) < F_m, \quad \phi(U_2) < F_m, \quad \phi(L_1) > F_M \quad \text{and} \quad \phi(L_2) > F_M.$$

Hence, L_1, L_2 and U_1, U_2 are, respectively, a pair of strict constant lower and upper solutions for (1).

Existence and Stability properties of T-periodic solutions: We remark that $g(t, x)$ and $g_x(t, x)$ verify the L^1-Carathéodory conditions on $[0, T] \times]0, \mu_1[$ because $h \in \mathcal{H}$ and $F \in C(\mathbb{R}/T\mathbb{Z})$.

As a consequence of Theorem 5.3 in [13] (chapter 1) and Remark 1 we obtain the existence of a T-periodic solution of (1), $x(t)$, such that for all $t \in \mathbb{R}$

$$L_2 < \ell_2 \leq x(t) \leq u_2 < U_2. \tag{16}$$

On the other hand, we have that $L_1 > U_1$ are a pair of strict constant lower and upper solutions of (1) and $g_x(t, x) \leq a(t)$ for all $(t, x) \in \mathbb{R} \times [U_1, L_1]$ where $a(t) \geq 0$ and is positive on a subset of positive measure. Now we shall apply Theorem 4.2 in [17] in order to obtain the conclusion. Notice it is not difficult to prove that Theorem 4.2 in [17] is valid whenever the x-domain is an open interval (see [20]). Moreover, (14) generalizes, for arbitrary periods T, the condition over the p-norm of a^+ in the set $\Omega_{p,c}$ defined in [17].

Besides, since the first step reveals that the number of non-trivial positive T-periodic solutions of (1) is finite, we have that all conditions to apply Theorem 4.2 in [17] are fulfilled and hence there exists a solution of (1), $v_0(t)$, which is asymptotically locally stable and verifies for all $t \in \mathbb{R}$ that

$$U_1 < v(t) < L_1. \tag{17}$$

Therefore $x(t)$ is the only T-periodic solution of (1) which verifies (16) and $v(t)$ is the only T-periodic solution of (1) which verifies (17). We conclude that $x(t)$ is unstable as a consequence of Proposition 3.1 and the subsequent Remark in [14] (see also Theorem 1.1 in [20]). □

Proof of Corollary 1. Notice that $F_m < F_M$ because F is non-constant and that $a(t) \geq 0$ for all $t \in \mathbb{R}$ by definition. We will prove that conditions (a) and (b) imply that (14) holds. Thus, under condition (a) we have $p = \infty$ so that $p^* = 1$ and $K(2p^*, T) = \frac{\pi^2}{T^2}$. Additionally, we have $F_M < \phi_M$ and

$$\frac{C_0}{2} - \frac{\pi^2}{2T^2}\left(1 + \frac{T^2 b^2}{4\pi^2}\right) < F_m,$$

where this last inequality implies that for all $t \in \mathbb{R}$

$$0 \leq a(t) = C_0 - 2F(t) \leq C_0 - 2F_m < \frac{\pi^2}{T^2}\left(1 + \frac{T^2 b^2}{4\pi^2}\right),$$

so that $|a(t)| < \frac{\pi^2}{T^2}\left(1 + \frac{T^2 b^2}{4\pi^2}\right)$ for all $t \in \mathbb{R}$. Hence (14) is satisfied for $p = \infty$. Now let us assume that (b) holds, then we have $p = 1$, $p^* = \infty$, $K(2p^*, T) = \frac{4}{T}$, $F_M < \phi_M$ and

$$\frac{1}{T}\int_0^T F(t)dt > \frac{C_0}{2} - \frac{2}{T^2}\left(1 + \frac{T^2 b^2}{4\pi^2}\right).$$

Hence

$$2\int_0^T F(t)dt > TC_0 - \frac{4}{T}\left(1 + \frac{T^2 b^2}{4\pi^2}\right),$$

which implies that

$$\int_0^T |a(t)|dt = TC_0 - 2\int_0^T F(t)dt < \frac{4}{T}\left(1 + \frac{T^2 b^2}{4\pi^2}\right),$$

so that (14) holds for $p = 1$. Therefore, an application of Theorem 2 with $p = \infty$ and $p = 1$ respectively finishes the proof. □

In order to proof Theorem 3 we need the following claim about the maximum value of the *auxiliary function* ϕ_α on the interval $]0, \mu_1[$ whenever $\alpha \in [0, \infty[$. We remark that if $\alpha = 0$ then we obtain a linear restoring force in the model (a canonical MEMS model, see [1]).

Claim 1. *Let $q(\alpha) := \phi_\alpha(c_\alpha)$ for $\alpha \in [0, \infty[$. Thus q is a monotone decreasing function.*

Proof of Claim 1. For each $\alpha \geq 0$, $c_\alpha \in]0, \mu_1[$ is the unique critical point of ϕ_α such that $\phi_\alpha(c_\alpha) = \max_{]0,\mu_1[} \phi_\alpha > 0$ (when $\alpha = 0$ we have $c_0 = \frac{1}{3}$ and $\phi_0(\frac{1}{3}) = \frac{4}{27}$). Furthermore, for $x \in]0, \mu_1[$ we have

$$\frac{\partial \phi_\alpha(x)}{\partial \alpha} = -x^2(1 - x)^2 < 0,$$

so that $\phi_{\alpha_2}(x) < \phi_{\alpha_1}(x) \leq \phi_{\alpha_1}(c_{\alpha_1})$ for all $x \in]0, \mu_1[$ and arbitrary $0 \leq \alpha_1 < \alpha_2$. We conclude that $q(\alpha_2) < q(\alpha_1)$. □

Proof of Theorem 3. A straightforward computation shows that $q(0) = \frac{4}{27}$, so from hypothesis and Claim 1 we have for $\alpha > 0$ that $2\beta V_{\max}^2 < 2\phi_\alpha(c_\alpha) = 2q(\alpha) < \frac{8}{27} < 1$. Since $h'(0) = 1$ we obtain by taking $F(t) = \beta V^2(t)$ that $C_0 = 1$. Thus (15) implies that condition (14) holds for $a(t) = 1 - 2\beta V^2(t)$. An application of Theorem 2 leads us to the conclusion. □

Proof of Corollary 2. Let us assume that (a) holds. Then $V_{max}^2 < \frac{\phi(\alpha)}{\beta}$ and

$$V_{min}^2 > \frac{1}{2\beta} - \frac{\pi^2}{2\beta T^2}\left(1 + \frac{T^2 b^2}{4\pi^2}\right).$$

Then

$$0 \leq 1 - 2\beta V^2(t) \leq 1 - 2\beta V_{min}^2 < \frac{\pi^2}{T^2}\left(1 + \frac{T^2 b^2}{4\pi^2}\right),$$

and hence (15) is satisfied for $p = \infty$. If we assume that now (b) holds we obtain that $\beta V_{max}^2 < \frac{\phi(\alpha)}{\beta}$ and

$$\int_0^T V^2(t)dt > \frac{T}{2\beta} - \frac{2}{\beta T}\left(1 + \frac{T^2 b^2}{4\pi^2}\right).$$

so that

$$T - \int_0^T 2\beta V^2(t)dt < \frac{4}{T}\left(1 + \frac{T^2 b^2}{4\pi^2}\right).$$

This last inequality implies that $\int_0^T |1 - 2\beta V^2(t)|dt < \frac{4}{T}\left(1 + \frac{T^2 b^2}{4\pi^2}\right)$ and then (15) holds for $p = 1$. An application of Theorem 3 finishes the proof. □

3. Some numerical results for a graphene-based MEMS model

In this section we present some numerical results for (2) and the comparison with the canonical parallel-plate MEMS model (Nathanson's model, see [1]), in order to highlight the advantages of using graphene.

Parameters values for the graphene MEMS model: Let E to denote the Young's modulus of the graphene, D the absolute value of the third order elastic stiffness modulus of graphene, A_c and L the cross-sectional area and the length of the graphene strip, m the mass of the movable plate, ϵ the dielectric constant of the gap medium, A the movable plate area, c the damping coefficient and d the initial gap between the plates. Then we have for (2) that

$$b = c\sqrt{\frac{L}{EA_c m}}, \quad \alpha = \frac{Dd}{EL} \quad \text{and} \quad \beta = \frac{\epsilon AL}{2EA_c d^3}.$$

Table 1 contains realistic values of the parameters that are employed to obtain the numerical results for the graphene-based MEMS model, when a voltage $V(t) = V_{DC} + V_{AC}\cos(\hat{\omega}t)$ is supplied. Notwithstanding, we notice that V_{DC} and V_{AC} can be tuned to convenience almost like "control parameters" to explore the dynamical behavior of the system as long as the required conditions of Theorem 3 or

Table 1
Parameters values.

β	$6.510\,432\,214\,911\,766 \times 10^{-4}$ /V^2
α	2.029411764705882e-02
b	1.153802627922852e-02
$\hat{\omega}$	6.806139097297727
T	9.231643986932663e-01

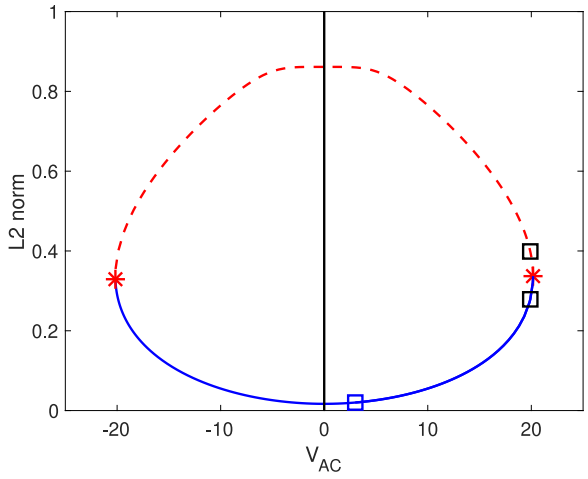

Fig. 2. Bifurcation diagram computed with AUTO using a pseudo arc length continuation scheme. The blue solid line is the stable part of the branch whereas the red dashed curve is the unstable one. The blue hollow square is the starting solution at $V_{AC} = 3$, the two black squares at $V_{AC} = 19.9$ are a stable (lower) and unstable (upper) solutions close to the limit point (red asterisks) where the branch changes its stability. (For interpretation of the references to color in this figure legend, the reader is referred to the web version of this article.)

Corollary 2 hold. Then we will consider $V_{DC} = 5\,\text{V}$ and $V_{AC} = 3\,\text{V}$, and then we will consider $V_{DC} = 3\,\text{V}$ and $V_{AC} = 1.5\,\text{V}$.

Numerical continuation results:

Here we present numerical continuation results as one of the parameters is changed using AUTO which is a well tested and powerful program to analyze (among others) periodic solutions of dynamical systems [21].

Fig. 2 shows the bifurcation diagram where the primary continuation parameter is the amplitude of the forcing V_{AC} for a fixed value of the DC voltage $V_{DC} = 5$ V. The blue hollow square at $V_{AC} = 3$ is the starting solution of the diagram which is stable and was computed numerically solving a boundary value problem with the parameters and boundary values inferred from part (a) in Corollary 2. As the branch (solid line) moves to higher values of V_{AC} the stability is preserved up to a critical value at which a limit point occurs (LP) (red asterisk). At this point the branch becomes unstable (dashed line) and the value of the continuation parameter diminishes until a vanishing value of the alternating voltage is reached. The vertical axis is the norm of the solution averaged over a period [21] and is just a scalar measure for the bifurcation diagram. Note that the equilibria for $V_{AC} = 0$ (one stable and another unstable) can be analytically computed for the autonomous case. The symmetric shape of the negative V_{AC} part of the bifurcation diagram is to be expected since the sign of alternating forcing does not play a role in the bifurcation behavior.

Two solutions close to the LP ($V_{AC} = 19.9$ (black squares)) has been selected and correspond to the stable and unstable solutions predicted by part (a) in Corollary 2. They will also appear in the stroboscopic Poincaré plot of the next section. The linear stability around these periodic solutions is measured by the corresponding Floquet multipliers and can be relevant for the applications.

Fig. 2 is a numerical implementation of part a) in Corollary 2: when the parameter lies in the appropriate interval we find two periodic solutions with opposite stability that live always in the positive part of x. Outside of the region no periodic solutions can be predicted and the separating case occurs exactly where the stable and the unstable periodic solution merge at a fold bifurcation.

In Fig. 3 we present the phase space representation of the positive solution exactly at the Limit Point in the bifurcation diagram.

We notice that the zoom close to the rightmost end of the curves shows a highly non symmetric and nonlinear behavior of the oscillation of the plate of the graphene MEMS. The solutions are always far enough from the singularity at $x = 1$.

Stroboscopic map: Now we present some results to illustrate the stability and basin of attraction associated to the positive T-periodic solution given by Corollary 1 which is asymptotically locally stable, through computation of the stroboscopic Poincaré map for the graphene-based MEMS. The stroboscopic maps were computed by accurately integrating forward and backwards in time with initial conditions close to the orbits of interest but keeping the position and velocity values only for integer time multiples of the period of the external forcing. We have used Matlab solver *ode45* with tolerances of the order of 10^{-14}.

The dynamical behavior of the trajectories can be visualized using two different color-maps with four colors each and two different time direction integrations. Color-bar A goes from green to blue and the trajectories remain one quarter of the time at each successive color in a forward time integration. The initial conditions for this case have been selected in a grid around to the stable equilibrium point. Color-bar B runs from yellow to red with the same convention (a quarter of the total time at each sub color) in a backwards time integration close to the unstable equilibrium point.

Fig. 4(a) shows the region of interest of the stroboscopic map when $V_{AC} = 19.9\,\text{V}$, with a mesh grid of 10200 nodes for the fixed point on the left, and a mesh grid of 1270 nodes for the fixed point on the right. Trajectories corresponding to the mesh grid of the fixed point on the left are portrayed with color-bar A, and those corresponding to the mesh grid of the fixed point on the right with the color-bar B. The integration in the first case was to 3000 T and in the second case was to −3000 T. Fig. 4(b) is a close up to the map that shows the existence of a region containing the fixed point on the left, for which the trajectories have an asymptotic behavior to that fixed point. This region also seems to be bounded by some of the trajectories corresponding to the mesh of the fixed point on the right. We notice the existence of trajectories that escape towards the singularity, resulting in a possible blow-up behavior.

A typical fish-like figure is formed around the stable–unstable equilibrium couple. As expected the green "fish" shrinks at the fold bifurcation and disappears. Note that from the applications point of view the region of interest is precisely the stable basin of attraction and the unstable initial conditions have to be avoided.

Fig. 5 shows the region of interest of the stroboscopic map when $V_{AC} = 4.5\,\text{V}$ by using the same color-maps as in the former case, a mesh grid of 10200 nodes with a perturbation parameter of 1.95e−02 for the fixed point on the left, and a mesh grid of 7675 nodes with a perturbation parameter of 3.46e−03 for the fixed point on the right. The conditions of Theorem 1 are satisfied, thus as the previous section shows, one of the positive T-periodic solutions is asymptotically locally stable and the other is unstable. Thus, we obtain the existence of a region of initial conditions for which trajectories have an asymptotic behavior to the fixed point on the left, moreover, this region is completely bounded by some of the trajectories with initial conditions nearby the fixed point of the right. Note that for this case the basin of attraction has increased significantly. This fact could be anticipated from the numerical continuation diagram 2 by looking at the distance between the two equilibria. In some sense the continuation and the stroboscopic diagrams provide complementary information about the dynamical behavior of the solutions.

Basin of Attraction Comparison: In this subsection we compare the basins of attraction (see [1]), of the two MEMS models, paying

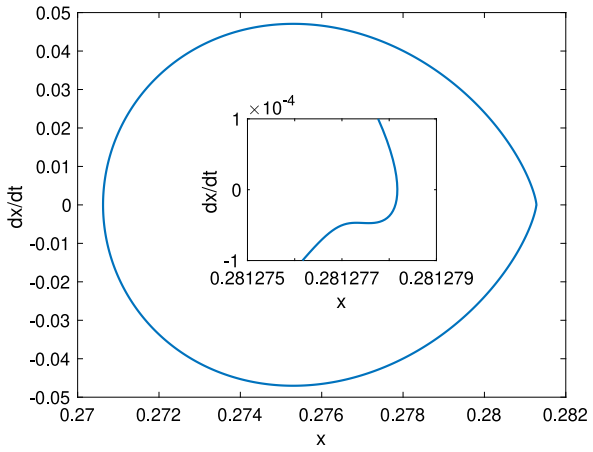

(a) Phase space representation of the positive solution at the Limit Point in the bifurcation diagram. The vertical axis is the velocity whereas the horizontal axis is the position. The inset is a zoom close to the rightmost part of the orbit.

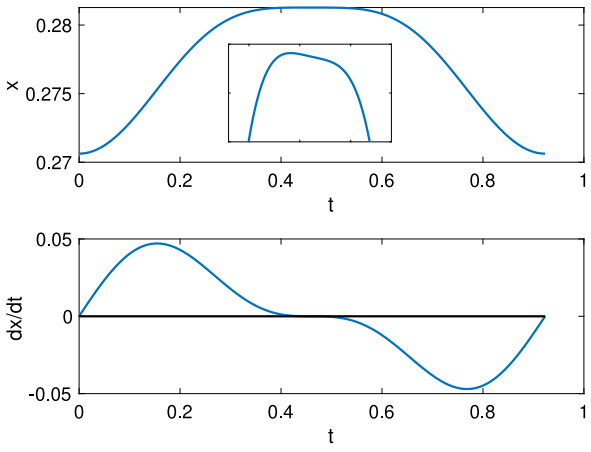

(b) Position (upper) with a zoom around the maximum value and velocity (lower) of the solution that is undergoing a Limit Point bifurcation.

Fig. 3. Phase space representation of the positive solution at the Limit Point in the bifurcation diagram, for this value of the V_{AC} parameter (20.1673) the stable and unstable solution merge.

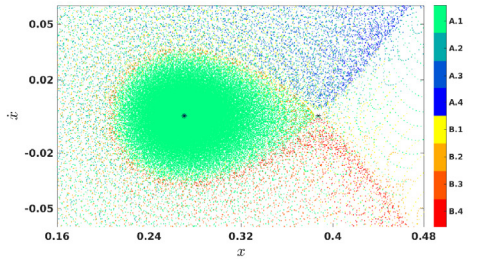

(a) Region of interest of the stroboscopic map with a typical fish-like figure.

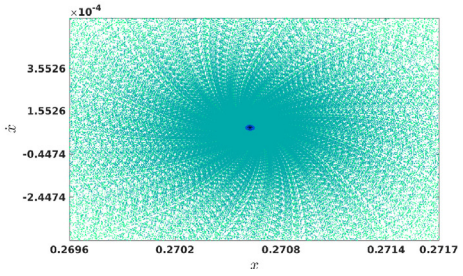

(b) Close up to the central region of the stroboscopic map.

Fig. 4. Region of interest of the stroboscopic map and close up associated to the case $V_{AC} = 19.9\,\mathrm{V}$. In 4(a) the desired experimental region is the green stable lobe around the stable periodic solution. A separatrix curve can also be observed separating the stable and unstable regimes. The unstable equilibrium point has two unstable and two stable directions. (For interpretation of the references to color in this figure legend, the reader is referred to the web version of this article.)

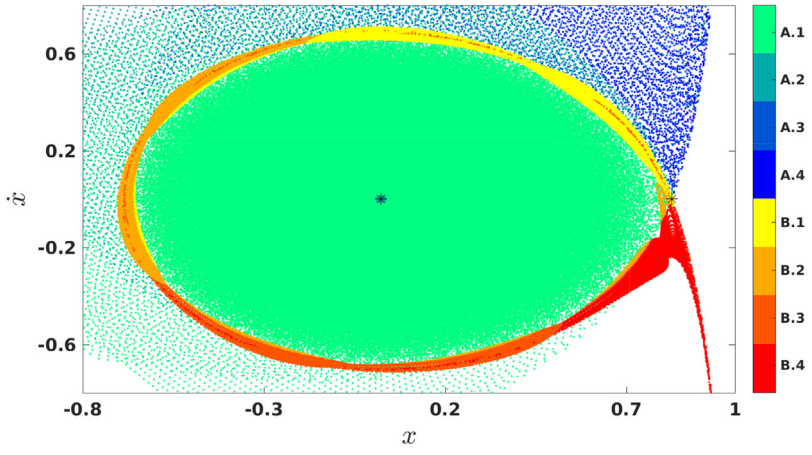

Fig. 5. Region of interest of the stroboscopic map associated to the case $V_{AC} = 4.5\,\mathrm{V}$.

special attention to the robustness properties. In order to tackle the comparison between the two models we need to ensure equivalent operating conditions. Therefore we will use in both models the same gap, area of the plates, damping coefficient, and the geometry of a parallel-plate device. Additionally, we will take into account for the Nathanson's model a linear restoration force as follows:

$$\overline{F}_{res} = -\overline{E} A_c \frac{x}{L},$$

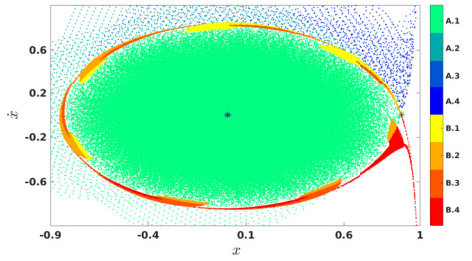

(a) Region of interest for the nonlinear response model.

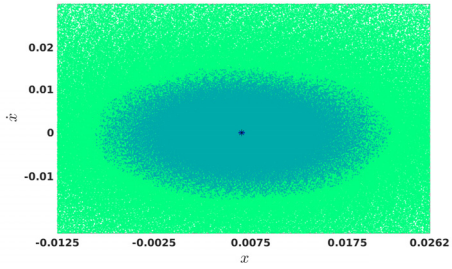

(b) Close up to the region of interest for the nonlinear response model.

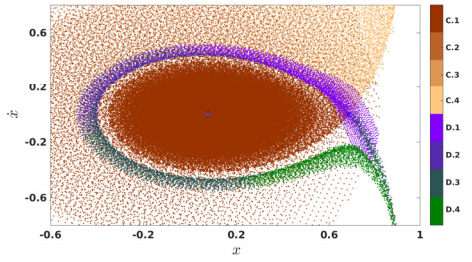

(c) Region of interest for the linear response model.

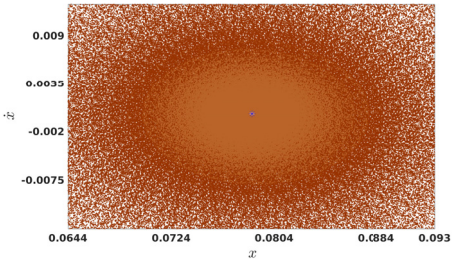

(d) Close up to the region of interest for the linear response model.

Fig. 6. Region of interest of the stroboscopic map associated to both models.

where A_c, L and x are defined as in Section 1, and $\overline{E}$ denotes the Young's modulus of some material, for example, the silicon. Hence we consider $\overline{E} = 100\,\text{GPa}$. On the other hand, to achieve the comparison we ensure the existence of two periodic solutions for the linear response model through the application of lower and upper solutions theorems, moreover, one of them is asymptotically locally stable. Before we present the results of this section we notice that the stroboscopic map associated to the linear response model has been shifted so that fixed points corresponding to the asymptotically locally periodic solutions for both models match.

We notice that for a periodic input voltage with $V_{DC} = 3\,\text{V}$ and $V_{AC} = 1.5\,\text{V}$, Figs. 6(a) and 6(c) show the region of interest of the stroboscopic map associated to both models. For the case of the nonlinear response model, we consider a mesh grid of 3720 nodes, and perturbation parameters of 3.305e−02 for the fixed point on the left and 3.065e−03 for the fixed point on the right. On the other hand, for the case of the linear response model we consider a mesh grid of 3720 nodes with a perturbation parameter of 3.06e−02 for the fixed point on the left, and a mesh grid of 1580 nodes with a perturbation parameter of 1.035e−02 for the fixed point on the right. Additionally, trajectories corresponding to the mesh grid of the fixed point on the left are portrayed with color-map C, and those corresponding to the mesh grid of the fixed point on the right with the color-map D. Fig. 6(b) is a close up to Fig. 6(a), and Fig. 6(d) is a close up to Fig. 6(c).

The size of the basin of attraction for the graphene-based MEMS is considerably larger than for the classical silicon based MEMS (please note the different scales).

Fig. 7 gives an insight into the comparison between the two models considering dimensional variables. We can observe that the set of initial conditions that leads to a good operation of the device, i.e., the safe operation region, of the model with nonlinear response is greater than the safe operation region of the model with linear response.

4. Concluding remarks

In this work we obtained results about the existence, multiplicity and the stability properties of lateral (positive) periodic oscillations of the movable plate in a family of MEM devices that are based on materials with elastic response verifying certain conditions (graphene and graphene-like materials), and which are modeled by Eq. (1). Moreover, we completed the study presented in [12] for the general Eq. (1) by showing analytically the occurrence of an asymptotically locally stable positive T-periodic oscillation. These results could be an approach to a design principle for stabilizing the device without an external controller, since a proper adjustment of the input voltage leads to the required behavior.

On the other hand, we found sufficient and precise conditions over control parameters that lead to the existence of lateral (positive) periodic oscillations and the existence of a stable and safe operation region in those graphene-based MEMS modeled by (2). Indeed, we showed that the role of the parameter α, which relates the elastic properties of the graphene with the geometry of the device, in the stabilization process of the device is merely to determine the associated "pull-in voltage" : $V_{max}^2 < \eta_2 := \eta_2(\alpha)$ (see [1] for more details) since the other conditions in Corollary 2 do not depend on α.

Regarding the gains of using graphene/graphene-like materials in MEMS with a simple parallel-plate capacitor configuration, we observe that under certain hypotheses on control parameters and ensuring the same operating conditions of devices, simulations show that the safe operation region (basin of attraction) of the graphene-based MEMS is greater than that of a canonical MEMS. Additionally, it is worthy to mention that although the structure of lateral (positive) oscillations seems to be preserved in both models, the pull-in voltage associated to the graphene-based MEMS is lesser than the pull-in voltage associated to that of a canonical MEMS as a consequence of the monotonically behavior of function q revealed by Claim 1. Hence, in practice we require a less voltage input in order to operate the graphene-based MEMS so these kind of devices could provide better performance at lower consumption.

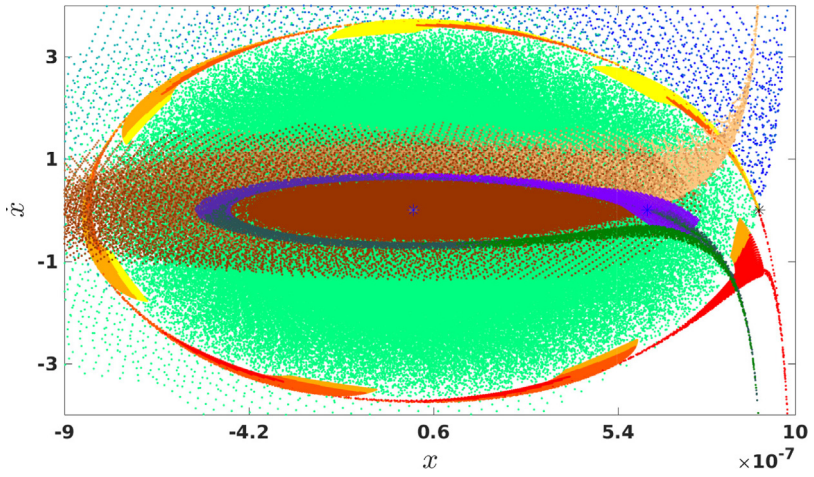

Fig. 7. Comparison between the regions of interest of the stroboscopic maps associated to the models with nonlinear and linear elastic response for $V_{DC} = 3\,\mathrm{V}$ and $V_{AC} = 1.5\,\mathrm{V}$.

Declaration of competing interest

The authors declare that they have no known competing financial interests or personal relationships that could have appeared to influence the work reported in this paper.

Data availability

Data will be made available on request.

Appendix. Some auxiliary results

This appendix contains some classical results which have been included for the benefit of the reader. The following Lemma provides information about the distance between consecutive zeros of solutions of a linear second order differential equation. This result is a consequence of the discussion in [18] about explicit criteria for the periodic maximum and antimaximum principles, and the adaptation of some well known ideas in [15] (see also [17] and [22]).

Lemma 3. *Consider $a \in L^1(0,T)$ and T-periodic. Assume that there exists $p \in [1,\infty]$ such that*

$$\|a^+\|_p < \left(1 + \frac{T^2 b^2}{4\pi^2}\right) K(2p^*, T),$$

where and p and p^* are conjugate exponents. Then the distance between two consecutive zeros of any non-trivial solution of

$$\ddot{u} + b\dot{u} + a(t)u = 0, \tag{A.1}$$

is greater than T. Moreover, if there exist $a_1(t)$ and $a_2(t)$ two functions enjoying the properties of $a(t)$ with

$$a_1 \ll a_2,$$

then the linear equations

$$\ddot{u} + b\dot{u} + a_i(t)u = 0,$$

for $i = 1, 2$ do not admit non-trivial T-periodic solutions simultaneously.

Next lemma provides a result on the multiplicity of non-trivial periodic solutions for a second order differential equation with finite domain (see [15] and [22]).

Lemma 4. *Consider the following second order differential equation*

$$\ddot{x} + b\dot{x} + g(t,x) = 0, \tag{A.2}$$

with $b > 0$ and $g : \mathbb{R}\times]x_1, x_2[\to \mathbb{R}$. Assume that $g \in C^{0,1}(\mathbb{R}/T\mathbb{Z}\times]x_1, x_2[)$, $g_{xx} < 0$ on $\mathbb{R} \times]x_1, x_2[$ and that there exists a T-periodic function $a(t)$ verifying the hypotheses in Lemma 3 such that for all $t \in \mathbb{R}$ and $x \in]x_1, x_2[$

$$g_x(t,x) \le a(t).$$

Then (A.2) has at most two non-trivial T-periodic solutions with range in $]x_1, x_2[$.

Proof. Let $u_1(t)$, $u_2(t)$ be a pair of different non-trivial T-periodic solutions of (A.2) with range in $]x_1, x_2[$, and let us define for each $t \in \mathbb{R}$

$$\zeta(t) = \begin{cases} \dfrac{g(t,u_2(t)) - g(t,u_1(t))}{u_2(t) - u_1(t)} & \text{if } u_2(t) \neq u_1(t), \\ g_x(t,u_2(t)) & \text{if } u_2(t) = u_1(t). \end{cases}$$

Then $\zeta \in C(\mathbb{R}/T\mathbb{Z})$ so that $\zeta \in L^1(0,T)$ and $w(t) = u_2(t) - u_1(t)$ is a non-trivial T-periodic solution of equation

$$\ddot{w} + b\dot{w} + a(t)w = 0. \tag{A.3}$$

Assume without loss of generality that for some fixed $t \in \mathbb{R}$, $u_1(t) < u_2(t)$, therefore from the Mean Value Theorem we have the existence of $u = u(t)$ such that $u \in]u_1(t), u_2(t)[$ and

$$\zeta(t) = g_x(t,u).$$

Hence, in general for each $t \in \mathbb{R}$ we have that there exists $u = u(t) \in]x_1, x_2[$ such that $\zeta(t) = g_x(t,u)$. From hypothesis over g_x we obtain that $\zeta(t) \le a(t)$ for all $t \in \mathbb{R}$, and since $\zeta^+ \le a^+$ it follows that

$$\|\zeta^+\|_p < \left(1 + \frac{T^2 b^2}{4\pi^2}\right) K(2p^*, T).$$

From the first part of Lemma 3 we obtain that w cannot vanish because it is a T-periodic function. Therefore $u_1(t) < u_2(t)$ or $u_2(t) < u_1(t)$ for all $t \in \mathbb{R}$.

On the other hand, let us assume that there exist $u_1(t)$, $u_2(t)$ and $u_3(t)$ non-trivial T-periodic solutions of (A.2). Then we can suppose that $u_1(t) < u_2(t) < u_3(t)$ for all $t \in \mathbb{R}$, take $\zeta(t)$ and $w(t)$ as before, and define

$$n(t) = \begin{cases} \frac{g(t,u_3(t)) - g(t,u_2(t))}{u_3(t) - u_2(t)} & \text{if } u_3(t) \neq u_2(t), \\ g_x(t,u_3(t)) & \text{if } u_3(t) = u_2(t). \end{cases}$$

Thus $n \in C(\mathbb{R}/T\mathbb{Z})$, $v(t) = u_3(t) - u_2(t)$ is a non-trivial T-periodic solution of equation

$$\ddot{v} + b\dot{v} + n(t)v = 0,$$

and from the Mean Value Theorem we get that for each $t \in \mathbb{R}$ exists $\underline{u} = \underline{u}(t) \in \left]u_1(t), u_2(t)\right[$, $\overline{u} = \overline{u}(t) \in \left]u_2(t), u_3(t)\right[$ such that $\zeta(t) = g_x(t, \underline{u})$ and $n(t) = g_x(t, \overline{u})$. Since $g_{xx} < 0$ on its domain and $\underline{u}(t) < \overline{u}(t)$ for all $t \in \mathbb{R}$ it follows that $\zeta(t) < n(t)$ for all $t \in \mathbb{R}$. From second part of Lemma 3 we conclude that either $w \equiv 0$ or $v \equiv 0$. Hence, (A.2) has at most two non-trivial T-periodic solutions. □

References

[1] M.I. Younis, MEMS Linear and Nonlinear Statics and Dynamics, Vol. 20, Springer Science & Business Media, 2011, http://dx.doi.org/10.1007/978-1-4419-6020-7.

[2] Z.H. Khan, A.R. Kermany, A. Öchsner, F. Iacopi, Mechanical and electromechanical properties of graphene and their potential application in MEMS, J. Phys. D: Appl. Phys. 50 (5) (2017) 053003, http://dx.doi.org/10.1088/1361-6463/50/5/053003.

[3] L.T. Le, M.H. Ervin, H. Qiu, B.E. Fuchs, W.Y. Lee, Graphene supercapacitor electrodes fabricated by inkjet printing and thermal reduction of graphene oxide, Electrochem. Commun. 13 (4) (2011) 355–358, http://dx.doi.org/10.1016/j.elecom.2011.01.023.

[4] H. Tian, T.-L. Ren, D. Xie, Y.-F. Wang, C.-J. Zhou, T.-T. Feng, D. Fu, Y. Yang, P.-G. Peng, L.-G. Wang, L.-T. Liu, Graphene-on-paper sound source devices, ACS Nano 5 (6) (2011) 4878–4885, http://dx.doi.org/10.1021/nn2009535.

[5] Y. Zhang, Y. Gu, Mechanical properties of graphene: Effects of layer number, temperature and isotope, Comput. Mater. Sci. 71 (2013) 197–200, http://dx.doi.org/10.1016/j.commatsci.2013.01.032.

[6] C. Martin-Olmos, H.I. Rasool, B.H. Weiller, J.K. Gimzewski, Graphene MEMS: AFM probe performance improvement, ACS Nano 7 (5) (2013) 4164–4170, http://dx.doi.org/10.1021/nn400557b.

[7] X. Zang, Q. Zhou, J. Chang, Y. Liu, L. Lin, Graphene and carbon nanotube (CNT) in MEMS/NEMS applications, Microelectron. Eng. 132 (2015) 192–206, http://dx.doi.org/10.1016/j.mee.2014.10.023.

[8] Y. Li, Reversible wrinkles of monolayer graphene on a polymer substrate: toward stretchable and flexible electronics, Soft Matter 12 (13) (2016) 3202–3213, http://dx.doi.org/10.1039/c6sm00108d.

[9] C. Lee, X. Wei, J.W. Kysar, J. Hone, Measurement of the elastic properties and intrinsic strength of monolayer graphene, Science 321 (5887) (2008) 385–388, http://dx.doi.org/10.1126/science.1157996.

[10] E. Cadelano, P.L. Palla, S. Giordano, L. Colombo, Nonlinear elasticity of monolayer graphene, Physical review letters 102 (23) (2009) 235502, http://dx.doi.org/10.1103/physrevlett.102.235502.

[11] A. Keşkekler, H. Arjmandi-Tash, P.G. Steeneken, F. Alijani, Symmetry-breaking-induced frequency combs in graphene resonators, Nano Letters 22 (15) (2022) 6048–6054, http://dx.doi.org/10.1021/acs.nanolett.2c00360, https://doi.org/10.1021/acs.nanolett.2c00360.

[12] S. Kadyrov, A. Kashkynbayev, P. Skrzypacz, K. Kaloudis, A. Bountis, Periodic solutions and the avoidance of pull-in instability in nonautonomous microelectromechanical systems, Math. Methods Appl. Sci. 44 (18) (2021) 14556–14568, http://dx.doi.org/10.1002/mma.7725.

[13] C. De Coster, P. Habets, Two-Point Boundary Value Problems: Lower and Upper Solutions, Vol. 205, Elsevier, 2006, http://dx.doi.org/10.1016/s0076-5392(06)x8055-4.

[14] E.N. Dancer, R. Ortega, The index of lyapunov stable fixed points in two dimensions, J. Dynam. Differential Equations 6 (4) (1994) 631–637, http://dx.doi.org/10.1007/bf02218851.

[15] J. Mawhin, Topological degree and boundary value problems for nonlinear differential equations, in: Lecture Notes in Mathematics, Springer Berlin Heidelberg, 1993, pp. 74–142, http://dx.doi.org/10.1007/bfb0085076.

[16] R. Ortega, Topological degree and stability of periodic solutions for certain differential equations, J. Lond. Math. Soc. s2-42 (3) (1990) 505–516, http://dx.doi.org/10.1112/jlms/s2-42.3.505.

[17] P.J. Torres, Existence and stability of periodic solutions of a duffing equation by using a new maximum principle, Mediterr. J. Math. 1 (4) (2004) 479–486, http://dx.doi.org/10.1007/s00009-004-0025-3.

[18] A. Cabada, J.Á. Cid, L. López-Somoza, Maximum principles for the Hill's equation, Elsevier/Academic Press, Amsterdam, 2018, xiii + 238.

[19] G. Talenti, Best constant in Sobolev inequality, Ann. Mat. Pura Appl. (4) 110 (1976) 353–372, http://dx.doi.org/10.1007/BF02418013.

[20] F.I. Njoku, P. Omari, Stability properties of periodic solutions of a duffing equation in the presence of lower and upper solutions, Appl. Math. Comput. 135 (2–3) (2003) 471–490, http://dx.doi.org/10.1016/s0096-3003(02)00062-0.

[21] B. Krauskopf, H.M. Osinga, J. Galán-Vioque (Eds.), Numerical Continuation Methods for Dynamical Systems, Springer Netherlands, 2007, http://dx.doi.org/10.1007/978-1-4020-6356-5.

[22] A. Gutiérrez, P. Torres, Nonautonomous saddle-node bifurcation in a canonical electrostatic mems, International Journal of Bifurcation and Chaos 23 (5) (2013) http://dx.doi.org/10.1142/S0218127413500880.